



# New flow simulation framework for underground hydrogen storage modelling considering microbial and geochemical reactions

A. Shojaee<sup>a,\*</sup>, S. Ghanbari<sup>a</sup>, G. Wang<sup>a</sup>, S. Gregory<sup>b</sup>, N. Dopffel<sup>c</sup>, E. Mackay<sup>a</sup>

<sup>a</sup> Institute of Geo Energy Engineering, Heriot-Watt University, Edinburgh, United Kingdom

<sup>b</sup> British Geological Survey, Keyworth, Nottingham, United Kingdom

<sup>c</sup> Norwegian Research Centre NORCE, Bergen, Norway

## ARTICLE INFO

### Keywords:

Underground hydrogen storage  
Microbial reactions  
Geochemical reactions  
Reactive transport modeling  
Energy transition

## ABSTRACT

The widespread use of hydrogen as an energy source relies on efficient large-scale storage techniques. Underground Hydrogen Storage (UHS) is a promising solution to balance the gap between renewable energy production and constant energy demand. UHS employs geological structures like salt caverns, depleted reservoirs, or aquifers for hydrogen storage, enabling long-term and scalable storage capacity. Therefore, robust and reliable predictive tools are essential to assess the risks associated with geological hydrogen storage. This paper presents a novel reactive transport model called “Underground Gas Flow simulATIons with Coupled bio-geochemical reactIons” or “UGFACT”, designed for various gas injection processes, accounting for geochemical and microbial reactions. The flow module and geochemical reactions in the UGFACT model were verified against two commercial reservoir simulators, E300 and CMG-GEM, showing excellent agreement in fluid flow variables and geochemical behaviour. A major step forward of this model is to integrate flow dynamics, geochemical reactions and microbial activity. UGFACT was used to conduct a simple storage cycle in a 1D geometry across three different reservoirs, each with different mineralogies and water compositions: Bentheimer sandstone, Berea sandstone, and Grey Berea sandstone, under three microbial conditions (“No Reaction”, “Moderate Rate”, “High Rate”). The findings suggest that Bentheimer sandstone and Berea sandstone sites may experience severe effects from ongoing microbial and geochemical reactions, whereas Grey Berea sandstone shows no significant H<sub>2</sub> loss. Additionally, the model predicts that under the high-rate microbial conditions, the hydrogen consumption rate can reach to as much as 11 mmol of H<sub>2</sub> per kilogram of water per day (*mmol / kg·day*) driven by methanogenesis and acetogenesis.

## 1. Introduction

A key bottleneck in energy transition is the mismatch between the intermittent nature of renewable energy sources like solar and wind, and the demand for energy. Hydrogen (H<sub>2</sub>), as a clean and efficient energy carrier, holds immense promise in enabling a sustainable energy future. [1,2]. The widespread adoption of H<sub>2</sub> as an energy source depends on efficient methods of large-scale storage. Underground Hydrogen Storage (UHS) utilizes geological formations including salt caverns, depleted reservoirs, and aquifers to store H<sub>2</sub>, offering long-duration and scalable storage capabilities. This enables the storage of excess renewable energy during periods of high generation for later use during low generation times, effectively balancing supply, and demand [3,4].

UHS faces several challenges that must be addressed for its successful

implementation, particularly when considering microbial and geochemical risks [5–7]. One key challenge is identifying suitable geological formations capable of safely storing H<sub>2</sub> without significant leakage or environmental impact, while also mitigating the potential for microbial consumption of the stored H<sub>2</sub> and subsequently the formation of corrosive byproducts like hydrogen sulphide (H<sub>2</sub>S) [8]. Assessing these formations for long-term storage can be complex and requires comprehensive geological, microbiological and engineering studies [9]. Additionally, ensuring the integrity of storage reservoirs over time, including managing potential issues such as subsurface pressure changes or aquifer contamination, is critical for maintaining safety and minimising operational risks [10–12]. Another challenge involves optimizing the efficiency and cost-effectiveness of UHS, including developing robust monitoring and control systems to detect and respond

\* Corresponding author.

E-mail address: [ashojaee19@gmail.com](mailto:ashojaee19@gmail.com) (A. Shojaee).

<https://doi.org/10.1016/j.ijhydene.2025.150453>

Received 11 May 2025; Received in revised form 25 June 2025; Accepted 9 July 2025

Available online 23 July 2025

0360-3199/© 2025 The Author(s). Published by Elsevier Ltd on behalf of Hydrogen Energy Publications LLC. This is an open access article under the CC BY license (<http://creativecommons.org/licenses/by/4.0/>).

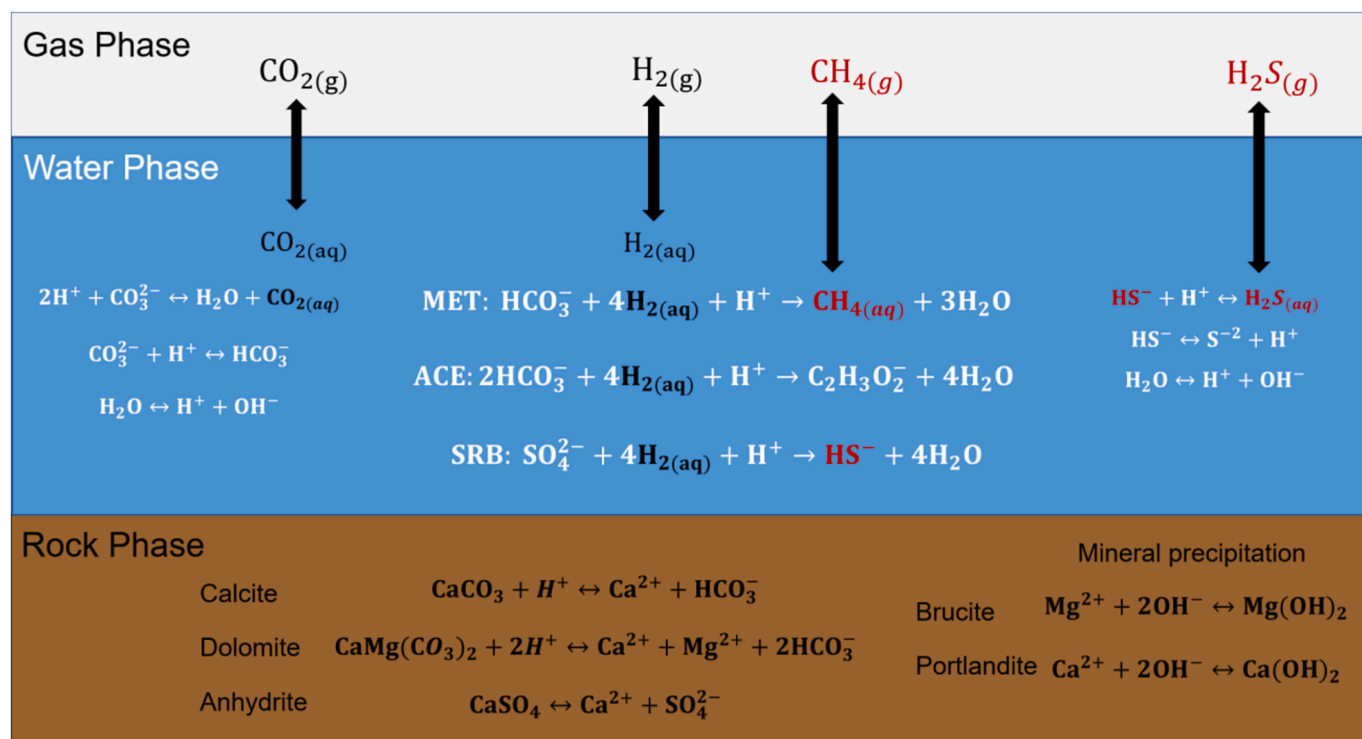


**Fig. 1.** In a porous medium, the introduction of  $\text{H}_2$  gas initiates its dissolution in water, potentially sparking microbial activity despite its limited solubility. This microbial utilization of dissolved  $\text{H}_2$  disturbs the equilibrium between the rock and fluid phases, leading to alterations in carbonate and sulphate concentrations and prompting compensatory rock dissolution. This sequence of events involving  $\text{H}_2$  dissolution, microbial activity, and rock dissolution results in the production of  $\text{CH}_4$  and  $\text{H}_2\text{S}$  [30].

to any potential leaks or integrity issues promptly [13,14]. Regulatory frameworks also need to be established to govern UHS operations, ensuring compliance with safety, environmental, and community impact standards [15]. Addressing these challenges, especially those related to microbial and geochemical risks, is essential to realize the full potential of UHS as a reliable and sustainable solution for large-scale  $\text{H}_2$  storage.

Microbial reactions such as methanogenesis, acetogenesis, and sulphate reduction can contribute to  $\text{H}_2$  loss in subsurface environmental conditions [16–19]. Hydrogenotrophic Methanogenesis (MET) involves certain Archaea that use  $\text{H}_2$  and carbon dioxide ( $\text{CO}_2$ ) to produce methane ( $\text{CH}_4$ ) as a metabolic byproduct. This process can lead to the loss of  $\text{H}_2$  [20] and contamination of stored  $\text{H}_2$ . Acetogenesis (ACE), carried out by acetogenic microorganisms, also utilizes  $\text{H}_2$  and  $\text{CO}_2$  to produce acetate ( $\text{CH}_3\text{COO}^-$ ) and involves the consumption of  $\text{H}_2$  [17,21,22]. Similarly, sulphate-reducing bacteria (SRB) use  $\text{H}_2$  as an electron donor to reduce sulphate ion ( $\text{SO}_4^{2-}$ ) to hydrosulphide ion ( $\text{HS}^-$ ) [21,23]. These microbial processes can significantly impact  $\text{H}_2$  storage systems, reduce overall storage efficiency and affect the performance of  $\text{H}_2$ -based technologies [24,25]. Understanding and mitigating these microbial reactions are crucial for optimizing  $\text{H}_2$  storage strategies and enhancing the utilization of  $\text{H}_2$  as a clean energy carrier.

Several studies have investigated this phenomenon from various perspectives, highlighting the importance of microbial reactions in the context of UHS. For example, Vítězová et al. [26] conducted an experimental study to evaluate the feasibility of the bio-methanation process in the presence of  $\text{H}_2/\text{CO}_2$  within *in-situ* brine and rock environments. The study observed a significant increase in the population percentage of methanogenic archaea from 1 % to 43 % by the 22nd day of the bottle test. Additionally, they reported complete metabolization of the stored gases within 42 days. In a recent purely numerical study by Hogeweg et al. [27] using the DuMu<sup>x</sup> simulator, it was highlighted that incorporating both geochemical and microbial reactions into the analysis results

in a considerably different  $\text{H}_2$  loss compared to simulation runs were these factors were not included because of  $\text{H}_2$  microbial and geochemical consumption. Such studies show that understanding the bio-geochemical aspects of UHS is crucial. Another study by Minougou et al. [28] presents a bio-reactive transport model for MET in UHS, focusing on the coupling of microbial kinetics with multiphase flow and gas transport. The model effectively captures the microbial conversion of  $\text{H}_2$  and  $\text{CO}_2$  into  $\text{CH}_4$  and demonstrates the importance of microbial processes in storage performance. While this work is an important contribution to the field, it does not explicitly consider mineralogical interactions or geochemical equilibria.

The integration of biological and geochemical reactions with fluid flow models represents a critical advancement in understanding and optimizing storage processes [29]. By incorporating biological reactions and geochemical reactions, including mineral dissolution and precipitation, into fluid flow models, it would be possible to simulate the complex interactions occurring within storage reservoirs more comprehensively. This integration allows for a holistic assessment of factors influencing storage performance, such as  $\text{H}_2$  consumption rates, pH evolution, and sulphide production. Moreover, by elucidating the dynamic interplay between microbial activity, geochemical reactions, and fluid behaviour, integrated models offer valuable insights for enhancing storage efficiency, mitigating operational risks, and ensuring long-term reservoir integrity in UHS applications [30].

Previously, our research delved into the interaction of biological and geochemical reactions within a batch model, revealing a significant interplay between microbial and geochemical reactions wherein microbial activity varied across different mineralogical systems [30,31]. In our present study, we aim to elevate our understanding by integrating the bio-geochemical model with a fluid flow model to propose a framework and develop a fully reactive model in the context of UHS. This integration will enable us to assess the coupling effects of fluid flow and reactions, thereby providing deeper insights into their coupled

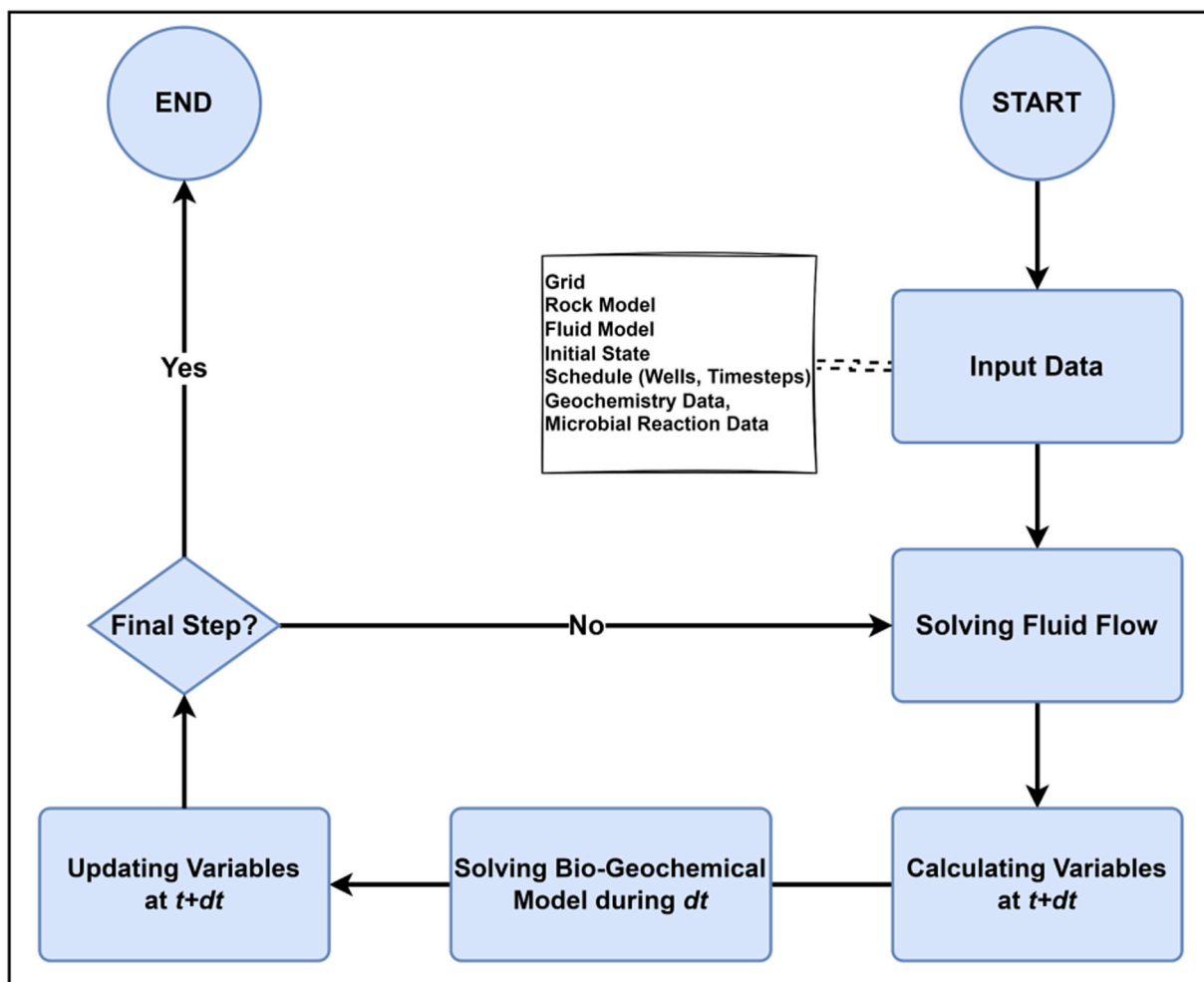


Fig. 2. General algorithm of coupling fluid flow model with the Bio-Geochemical model.

dynamics.

## 2. Methodology

### 2.1. Batch model description

The batch model, developed using PHREEQC [32], serves as a tool in simulating the complex interplay between biological and geochemical processes within UHS systems. In this model, all geochemical reactions are assumed to be at equilibrium, while microbial reactions are governed dynamically by a rate-based approach. Porosity changes due to mineral dissolution and precipitation were incorporated into the model. The corresponding impact on permeability was calculated using the Carman–Kozeny relationship, which links permeability to porosity changes.

Three microbial processes—MET, ACE, and SRB—are included to evaluate their importance in UHS [30]. Fig. 1 shows how the introduction of H<sub>2</sub> into the *in-situ* fluids may trigger some microbial reactions and disrupt the equilibrium between rock and fluid.

Input parameters such as brine composition, rock mineralogy, gas composition and kinetic data for microbial reactions, alongside pressure and temperature, are key parameters influencing the model's dynamics. In particular, microbial reactions are sensitive to variations in pH, temperature, and salinity. To this end, a quadratic equation is employed to generate a correction factor, modulating microbial reaction rates based on prevailing environmental conditions. This correction factor ensures that microbial activity is accurately reflected across a spectrum

of pH, temperature, and salinity fluctuations, thereby enhancing the model's predictive capabilities [30].

To incorporate both microbial and geochemical reactions into a PHREEQC model based on the outlined assumptions, it is necessary to decouple the PHREEQC database. Within the utilized database, the reduction of carbonate and sulphate by H<sub>2</sub> is treated as an equilibrium reaction. While integrating the kinetics of mineral dissolution/precipitation into the model is relatively straightforward, incorporating kinetics into aqueous phase reactions presents a different challenge. This involves decoupling and redefining reactions for carbonate (C(4)), methane (C(-4)), sulphate (S(6)), and sulphide (S(-2)) species with new notations, excluding those reactions governed by kinetics. Subsequently, the desired reactions are defined using kinetic keywords. Examples 9 and 15 in the PHREEQC manual illustrate this process for clarity [32, 33].

In the developed model, microbial reaction rates are calculated by a well-established rate model, named Dual-Monod [34–37], as follows:

$$r_s = -\frac{\mu_{max}}{Y} \frac{C_D}{K_D + C_D} \frac{C_A}{K_A + C_A} X \quad 1$$

$$r_x = -Yr_s - bX \quad 2$$

where  $r_s$  is substrate consumption rate ( $mol/sec$ ),  $\mu_{max}$  is specific growth rate ( $1/sec$ ),  $X$  is amount of biomass ( $mol$ ),  $Y$  is yield coefficient ( $mol X/mol H_2$ ),  $C$  is concentration ( $mol/L$ ),  $A$  and  $D$  refer to Electron Acceptor and Electron Donor,  $K$  is half-saturation constant ( $mol/L$ ),  $r_x$  is

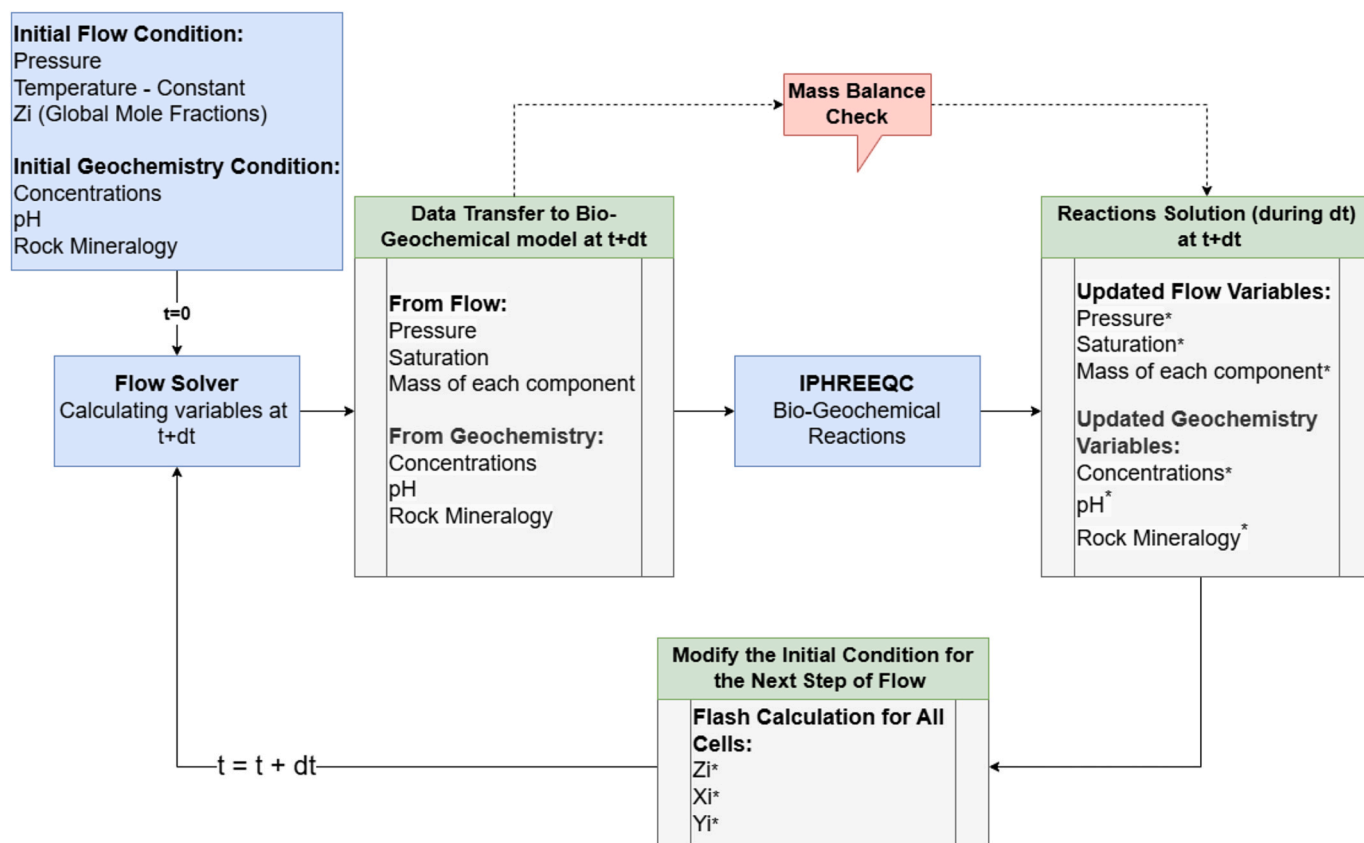


Fig. 3. Flowchart of the coupled fluid flow and bio-geochemical simulation process.

Table 1

The input data for CO<sub>2</sub> injection scenario.

Reservoir Dimensions	100 m × 50 m × 20 m
Grid Dimensions	50 × 1 × 1
Porosity	20%
Permeability	100 mD
Initial Pressure	150 bar
Temperature (constant)	90 °C
Initial Global Mole Fraction	Z <sub>H2O</sub> = 99%, Z <sub>CH4</sub> = 1%, Z <sub>CO2</sub> = 0%
Initial Water Saturation (Equivalent to the initial water mole fraction at reservoir condition)	93.45%
CO <sub>2</sub> -H <sub>2</sub> O Binary Interaction Coefficient	-0.04
CH <sub>4</sub> -H <sub>2</sub> O Binary Interaction Coefficient	-0.12
CO <sub>2</sub> -CH <sub>4</sub> Binary Interaction Coefficient	0
Reservoir Mineralogy	CaCO <sub>3</sub>

rate of biomass change ( $mol/sec$ ), and  $b$  is decay coefficient ( $1/sec$ ).

It is assumed that all three metabolisms are active at the same time. The details of the batch model and its assumptions are published previously [30].

### 2.2. Fluid flow model

In this study, we utilized the MATLAB Reservoir Simulation Toolbox (MRST) due to its open-source nature, which facilitates the development and testing of new models tailored to our specific needs [38]. We specifically employ the compositional module to conduct detailed compositional gas-water simulations based on the Peng-Robinson Equation of State (EOS) [39]. Gas solubilities in the liquid water phase are driven by the EOS, ensuring precise modeling of phase behavior and interactions between gas and water. Additionally, the use of Binary Interaction Coefficients (BICs) allows us to tune gas solubilities, enhancing the

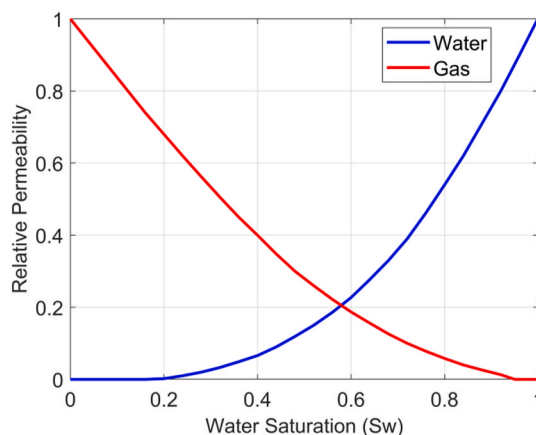


Fig. 4. Relative permeability curves.

accuracy and reliability of the simulation results. This approach enables a deeper understanding of the multiphase flow dynamics within the reservoir, ultimately aiding more effective reservoir management and development strategies. This compositional module enables the simulation of Underground Gas Storage (UGS) scenarios by considering multiple components, such as water (H<sub>2</sub>O), H<sub>2</sub>, CO<sub>2</sub>, H<sub>2</sub>S and CH<sub>4</sub>. This capability is crucial for modeling realistic UGS scenarios, where the interaction and behavior of these components under varying reservoir conditions need to be understood comprehensively.

### 2.3. Coupling algorithm

The flowchart presented in Fig. 2 outlines the simulation procedure

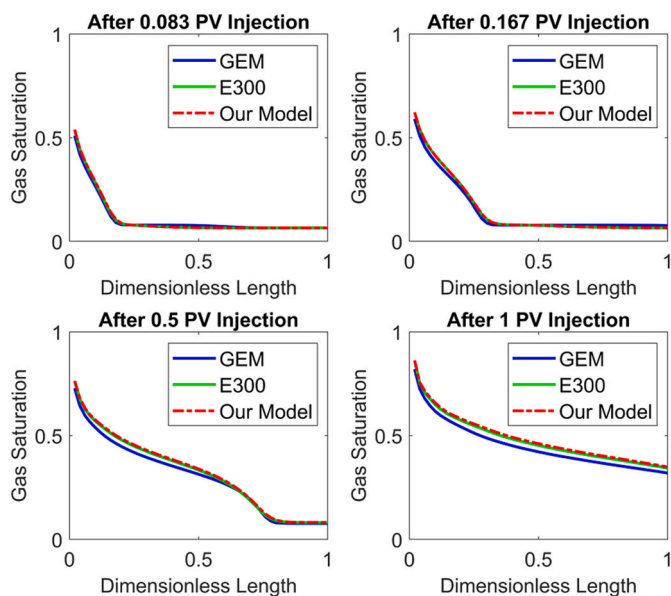


Fig. 5. Gas saturation profiles after 0.083, 0.167, 0.5, and 1 PV CO<sub>2</sub> injection.

designed to model the dynamic interactions in a system involving bio-geochemical reactions and fluid flow. The procedure begins with the initialization of input data, setting up the initial conditions - including pressure, temperature, and compositions, and also equilibrating rock and fluid properties in terms of geochemistry – all required for the simulation. Following this, the transport equation is solved, which involves determining the distribution and movement of fluids within the system (a single step of compositional simulation). Once the flow equation is solved, variables are calculated for the next time step ( $t + dt$ ), where  $dt$  represents the incremental time step in the simulation.

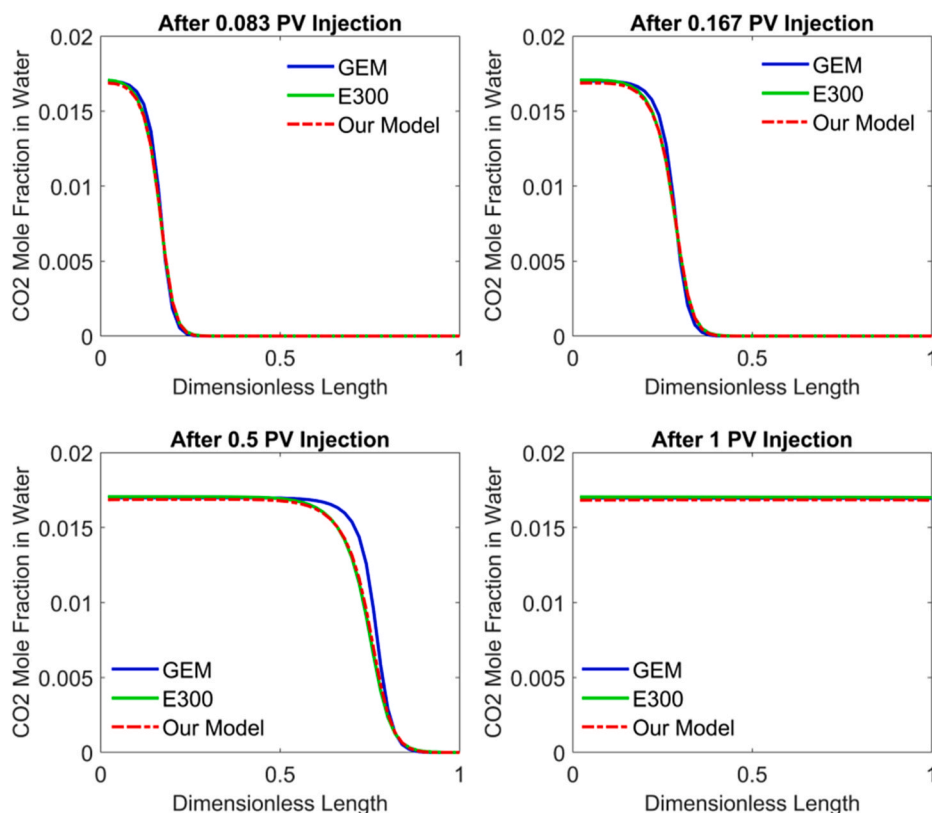


Fig. 6. Profiles of dissolved CO<sub>2</sub> after 0.083, 0.167, 0.5, and 1 PV CO<sub>2</sub> injection.

Next, the bio-geochemical calculations for each cell are solved in PHREEQC. The variables are then updated to reflect the changes resulting from the reactions. The procedure loops back to continue until the simulation terminates. This new approach serves as a useful tool by coupling flow dynamics with biochemical and geochemical processes. It can provide valuable insights into the biogeochemical processes and their impact on gas-water flow within the reservoir [40].

Fig. 3 illustrates the detailed functioning of the model. The flow model addresses the transport equation for a compositional system and implicitly calculates the primary variables, including pressure, global mole fraction, and well variables. Subsequently, the pressure, mass of each component (derived from mole fractions and density), and volumes (saturations) are used as input for calculations in PHREEQC. A series of batch calculations is then performed for each cell independently and in parallel. Based on the reactions, the variables are updated and used as initial conditions for the next time step in the flow model. This iterative algorithm continues until the final timestep is reached.

The main challenge in this context is managing two flash engines: one within the flow model and another within the biogeochemical model. This dual system can lead to inconsistencies between the models. MRST's compositional module relies entirely on the EOS, here treating water as the liquid phase and calculating mole fractions in both liquid and vapor phases using the EOS and iso-fugacity assumption. In contrast, PHREEQC calculates gas solubilities based on Henry's Law and applies the EOS only to the gas phase. To address this issue, we adjusted the Binary Interaction Coefficients (BICs) in the flow model's flash engine, tuning it to closely match the solubility results from Henry's Law. This approach ensures that the recalculated mole fractions are consistent before integrating them into the flow model. Additionally, it is crucial to monitor the mass balance as data is transferred between the two engines.

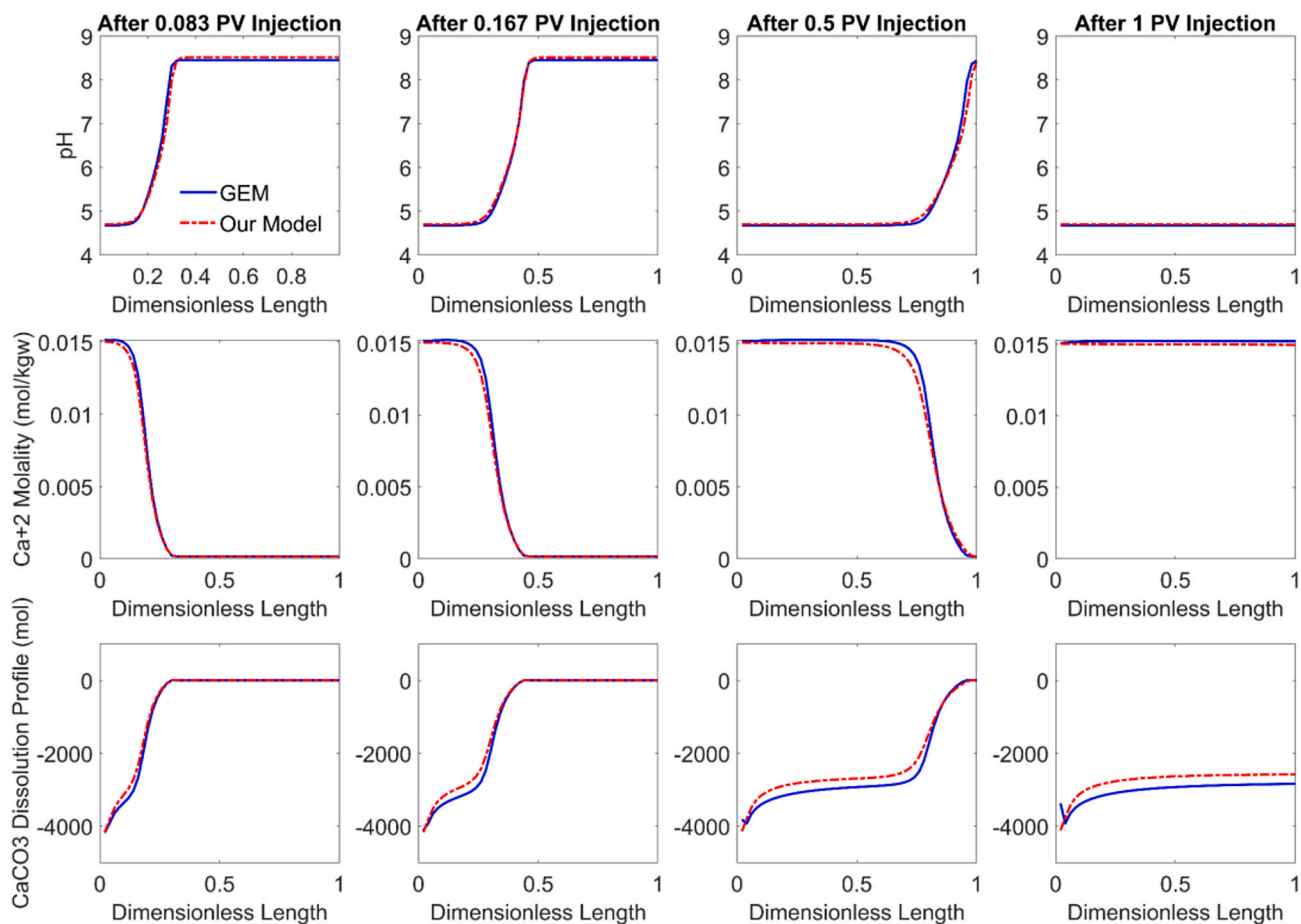


Fig. 7. Comparison between GEM and our model of pH,  $\text{Ca}^{+2}$  molality, and  $\text{CaCO}_3$  dissolution-precipitation profiles during  $\text{CO}_2$  injection. The amount of calcite dissolution is up to 0.01 % of the presented mineral in each grid block.

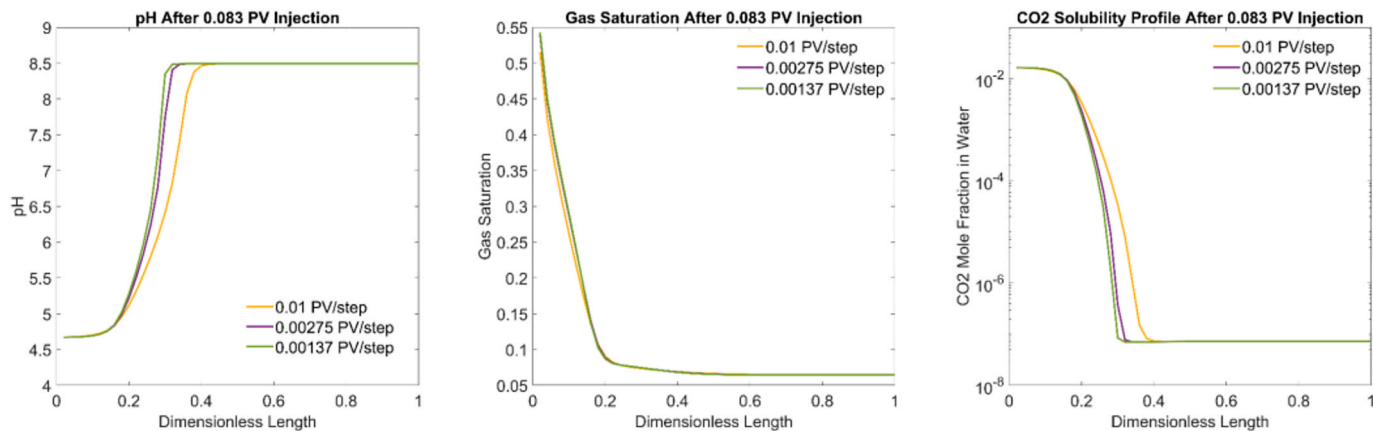


Fig. 8. Sensitivity analysis on time step size.

### 3. Results and discussion

#### 3.1. Model benchmarking

The proposed coupled model (named “Underground Gas Flow Simulations with Coupled Bio-Geochemical Reactions” or “UGFACT”) is designed to account for geochemical reactions at equilibrium and biological reactions governed by a rate model (kinetics). As the geochemical reactions are faster than microbial reactions, we tested a scenario in which geochemical reactions are governed by a rate model as well as

microbial reactions, and we observed no difference in results.

By setting the rate of microbial reactions to zero, the model should exclusively predict geochemical behaviour. To validate the model, a  $\text{CO}_2$  injection case is constructed to compare our model’s results with those from CMG-GEM (GEM) and ECLIPSE 300 (E300), both of which are commercial reservoir simulators for compositional modelling. Additionally, GEM can model geochemical reactions while simulating compositional fluid flow. Both UGFACT and GEM used the same equilibrium constant for calcite ( $\text{CaCO}_3$ ) at the specified temperature. For the kinetic rate constant and specific surface area in GEM, we used

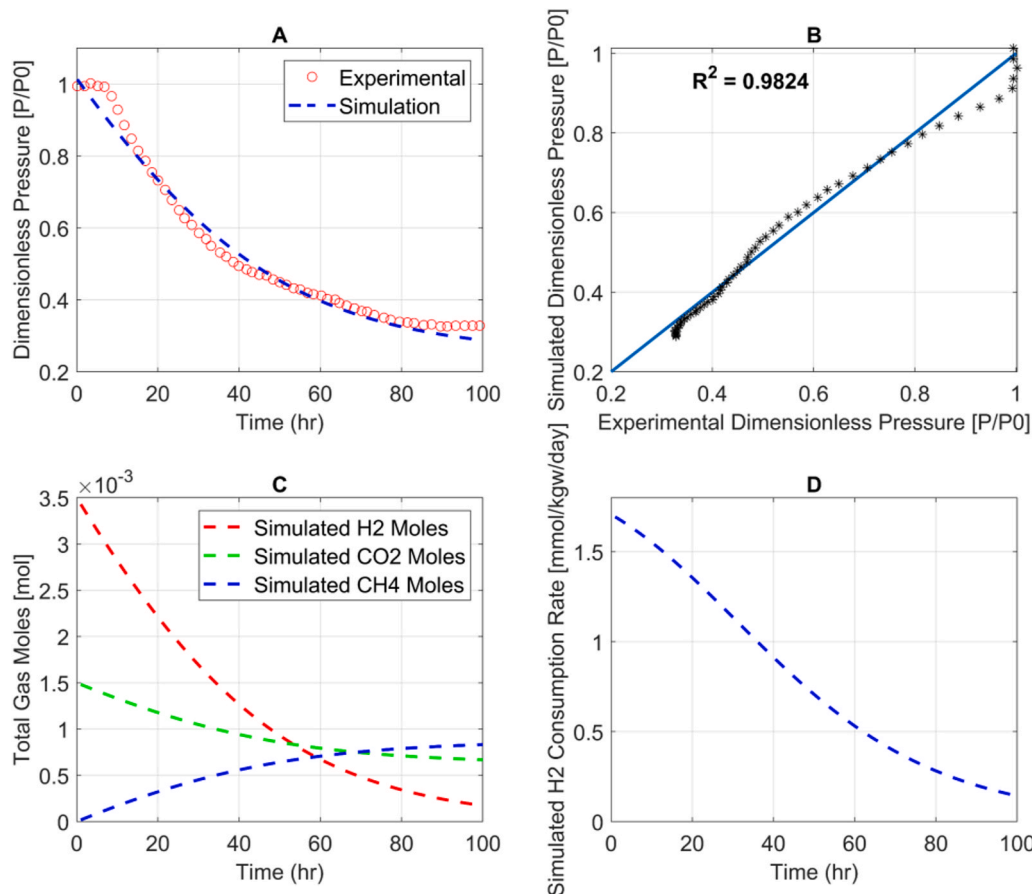


Fig. 9. Benchmarking of the microbial methanogenesis model against experimental data from Strobel et al. [42].

Table 2  
Matched parameters.

	$\mu_{max}$ (day <sup>-1</sup> )	$N_0$ (cell/ ml)	$K_D$ (mmol/ L)	$K_A$ (mmol/ L)	$Y$
Strobel et al. [42]	0.864	4.3e8	0.02	0.011	0.03 (mol Biomass/mol H <sub>2</sub> )
UGFACT	1.13	1.06e8	0.61	0.61	1e11 (cell/mol H <sub>2</sub> )

Table 3

Reservoir mineralogies that are used in the simulations. It is assumed that there are two main minerals in addition to quartz and other non-reactive minerals, and the non-reactive minerals do not interact with the fluids.

Storage Site	Mineral Weight Percentage (%)		
	Calcite	Dolomite	Quartz + Inert Minerals
A: Bentheimer sandstone [43]	0	2	98
B: Berea sandstone [44]	2	1	97
C: Grey Berea sandstone [45]	2	0	98

typical values reported in the literature. The final extent of dissolution is primarily governed by the equilibrium constant and the chosen activity model; in our case, the Debye-Huckel model was applied.

A 1D model saturated with brine (we used fresh water and equilibrated it with calcite to create initial brine composition) and CH<sub>4</sub> is assumed. CO<sub>2</sub> is injected from the left side of the model for 1 Pore Volume (PV) at reservoir thermodynamic conditions, and there is a

producer with constant Bore Hole Pressure (BHP) condition at the initial pressure of the reservoir. Table 1 shows the input data to construct the benchmark simulation case. Also, Fig. 4 presents the relative permeability used in the simulations.

Figs. 5 and 6 present comparisons of gas saturations and CO<sub>2</sub> mole fractions in water at four different times, using three models: GEM (blue line), E300 (green line), and our proposed model (red dashed line). The four subplots in each figure correspond to different stages of injection: after 0.083 PV, 0.167 PV, 0.5 PV and 1 PV injection.

The results demonstrate that our proposed model shows an excellent agreement with both GEM and E300 in terms of gas saturation across all stages of injection. At early stages (0.083 PV and 0.167 PV), all three models display similar saturation profiles with minor discrepancies. As the injection progresses (0.5 PV and 1 PV), the saturation profiles continue to exhibit strong agreement, highlighting the rigor of our model in simulating gas saturation behavior. Similarly, the comparison of CO<sub>2</sub> mole fraction in water reveals that our proposed model closely aligns with both GEM and E300 across all stages of injection. This consistent performance in both gas saturation and CO<sub>2</sub> solubility underscores the reliability and robustness of our proposed model when compared to established commercial simulators for simulating the physical interaction between CO<sub>2</sub> and water during injection processes.

The charts displayed in Fig. 7 compare pH, Ca<sup>+2</sup> molarity, and CaCO<sub>3</sub> dissolution profiles at different times, using GEM and our developed model. The alignment of the results from both models across all plots indicates a high degree of agreement, demonstrating the accuracy and reliability of the new model in simulating the geochemical processes under study. The consistent overlap between the curves suggests that our model can effectively replicate the outcomes produced by GEM, providing validation for its use in similar geochemical simulations. A minor discrepancy is observed in the late-time calcite dissolution profile,

**Table 4**

Brine composition when equilibrated with the given minerals.

Storage Site	Brine Data [45] - Equilibrated with the storage site mineralogy						pH
	Cations Molality (mol/kg)			Anions Molality (mol/kg)			
	Na <sup>+</sup>	Ca <sup>2+</sup>	Mg <sup>2+</sup>	Cl <sup>-</sup>	SO <sub>4</sub> <sup>2-</sup>	HCO <sub>3</sub> <sup>-</sup>	
<b>A: Bentheimer sandstone</b>	2.865	0.2857	0.1143	3.655	4.664e-03	1.119e-03	6.24
<b>B: Berea sandstone</b>	2.865	0.2920	0.1093	3.655	4.664e-03	4.401e-03	5.96
<b>C: Grey Berea sandstone</b>	2.865	0.3206	0.0802	3.655	4.664e-3	3.836e-3	5.95

**Table 5**

Microbial reaction rate parameters taken from literature. Two specific growth rates are used to reflect moderate and high microbial conditions.

Metabolism	$\mu_{max}(\text{day}^{-1})$	$K_D(\mu\text{M})$	$K_A(\mu\text{M})$	$Y(\frac{\text{molX}}{\text{molH}_2})$	$b(\text{day}^{-1})$
MET	Moderate: 1.109 High: 4.1 [48]	2-16 [48] Average: 9	230 [47]	0.03 [34]	0.01 * $\mu_{max}$
ACE	Moderate: 0.872 High: 1.9 [49]	1.3-3.7 [50] Average: 2.5	1-230 [47] Average: 115.5	0.07 [34]	
SRB	Moderate: 1.048 High: 5.5 [48]	1.8-4 [48] Average: 2.9	3-5500 [51] Average: 2751.5	0.08 [34]	

**Table 6**

The input data for UHS scenarios.

Reservoir Dimensions	50 m × 1 m × 1 m
Number of cells	50 × 1 × 1
Porosity	20%
Permeability	100 mD
Initial Pressure	150 bar
Temperature (constant)	60 °C
Initial Global Mole Fraction	Z <sub>H2O</sub> = 90%, Z <sub>CH4</sub> = 10%
Initial Water Saturation (Equivalent to the initial water mole fraction at reservoir condition)	55.08%
CO <sub>2</sub> -H <sub>2</sub> O Binary Interaction Coefficient	-0.04
CH <sub>4</sub> -H <sub>2</sub> O Binary Interaction Coefficient	-0.12
H <sub>2</sub> -H <sub>2</sub> O Binary Interaction Coefficient	-0.58
H <sub>2</sub> Injection Rate	6.2811 m <sup>3</sup> /day (equivalent to 0.005 PV/day)
Producer Constraint	Flow Rate = 6.2811 m <sup>3</sup> /day (equivalent to 0.005 PV/day) with BHP Limit = 150 bar

where the GEM results indicate CaCO<sub>3</sub> precipitation due to water evaporation and supersaturation. However, our model does not account for water evaporation at this stage, which may explain this deviation.

Overall, the high degree of concordance between the two sets of results validates the new model's efficacy in capturing the complex interactions and dynamics of geochemical processes in porous media. This validation is crucial for establishing the model as a reliable tool for simulating subsurface flow and reactive transport, providing confidence in its application for future studies and practical implementations. The successful benchmarking against GEM highlights the new model's potential to contribute significantly to advancements in understanding and predicting geochemical behaviour in subsurface environments.

The results suggest that this modeling approach offers a simple yet robust method for simulating reactive transport phenomena. However, an important limitation arises concerning the choosing of the time step size. This method presumes no reaction during fluid flow, with the effects of reactions applied after solving the transport equation. Consequently, our ability to select larger time steps is restricted, demanding consideration to stability when discretising time. To assess the impact of time step size, a sensitivity analysis was conducted. Fig. 8 demonstrates the impact of time step size on flow and geochemistry predictions of the model. The three panels display pH (left), gas saturation (middle), and CO<sub>2</sub> mole fraction (right) profiles. The model is discretized based on the fraction of pore volume injected per time step, represented by different

coloured curves in each panel. While larger time steps generally increase numerical dispersion, causing a more advanced front in some cases [41], here the gas saturation front remains mostly unaffected by time step changes. In contrast, the pH front shows a notable impact, with smaller time steps producing a sharper transition. This effect is particularly significant for geochemical properties, where small changes in concentration (here CO<sub>2</sub> concentration) can lead to substantial pH shifts. This pH behavior is directly influenced by numerical dispersion in CO<sub>2</sub> solubility calculations, as small changes in dissolved CO<sub>2</sub> concentration can lead to substantial changes in pH.

Moreover, validated the microbial reaction component using experimental data published by Strobel et al. [42]. In their study, H<sub>2</sub> and CO<sub>2</sub> were introduced into a bioreactor containing methanogenic microbes, and the resulting pressure drop was monitored over time, reflecting the net reduction in gas moles due to MET. To replicate this behaviour, we designed a similar setup by exposing 0.0035 mol of H<sub>2</sub> and 0.0014 mol of CO<sub>2</sub> to 1 kg of water (similar to that study), allowing us to assess the kinetics of MET under controlled conditions.

Fig. 9 presents the benchmarking of the microbial methanogenesis model against experimental data from Strobel et al. [42]. Panel A shows the dimensionless pressure decline over time, where the simulation closely follows the experimental trend, indicating good agreement. This is further confirmed in Panel B, which compares simulated and experimental pressures on a 1:1 line, yielding an R<sup>2</sup> value of 0.9824. Panel C illustrates the consumption of H<sub>2</sub> and CO<sub>2</sub> with production of CH<sub>4</sub>, consistent with methanogenic stoichiometry. Panel D shows the decreasing H<sub>2</sub> consumption rate, reflecting substrate depletion and the system's approach to equilibrium. The pressure behaviour was matched by performing a global optimization to minimize the error between simulated and experimental data. Overall, the results demonstrate that the model captures the microbial dynamics and pressure response with high accuracy.

The matched specific growth rate in our model is 1.13 day<sup>-1</sup>, compared to 0.864 day<sup>-1</sup> reported by Strobel et al. [42]. In addition to the growth rate, we also calibrated the initial biomass concentration as well as the half-saturation constants for the electron donor (K<sub>D</sub>) and electron acceptor (K<sub>A</sub>). These parameter values are presented in Table 2. The differences from the values reported by Strobel et al. stem from key distinctions between the two modelling approaches. First, our model does not include explicit formulations for lag or linear growth phases. Second, pH directly influences the reaction rate in our formulation, as detailed in the methodology. Lastly, not all experimental conditions and controlling factors from the original study were available to us. Nevertheless, the strong agreement between the simulated and experimental

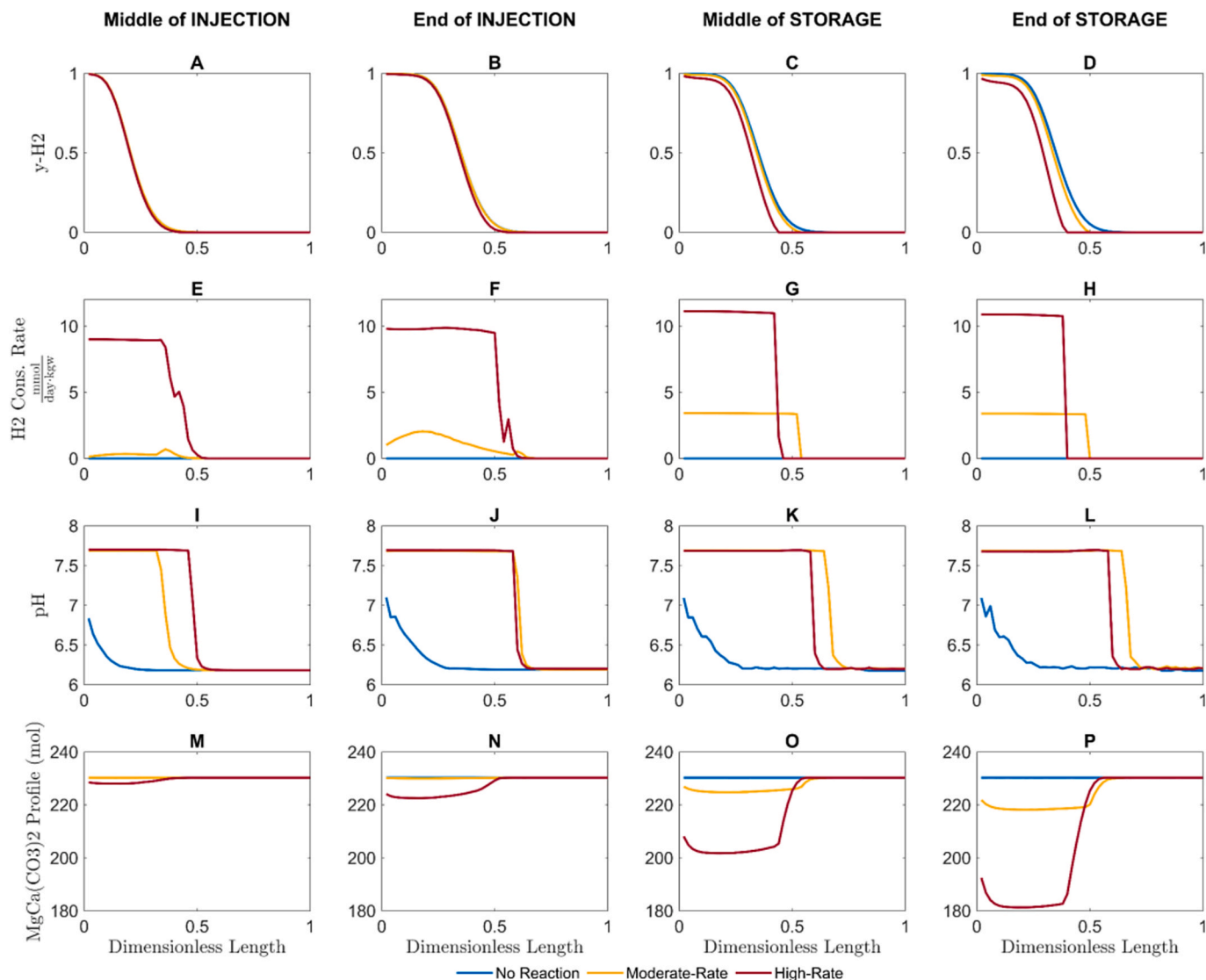


Fig. 10. Simulation results during the injection and storage period in site A with Bentheimer sandstone.

pressure profiles demonstrates that our model is capable of reliably representing methanogenesis under relevant conditions.

### 3.2. Bio-geochemical behavior during UHS – A simple case study

To investigate the biochemical and geochemical behavior under fluid flow conditions, we can employ the developed model to simulate a complete storage cycle. This involves designing a straightforward storage scenario where a one-dimensional horizontal reservoir, initially saturated with water and  $\text{CH}_4$ , is used.  $\text{H}_2$  is then injected for a 50-day period, followed by 150 days of shut-in during storage. Finally, the same well is used to back-produce  $\text{H}_2$  for 50 days. A set of simulations is designed to investigate UHS performance in three different mineralogies with three different choices of microbial reaction rates which are: I) No Reaction, II) Moderate-Rate, and III) High-Rate. Table 3 and 4 present the geochemistry conditions (rock mineralogy and brine composition) of each storage site taken from the literature [43–45]. The lack of reliable kinetic parameters for microbial reactions presents a major challenge in accurately modeling these processes. Conducting targeted experiments under UHS conditions is essential to obtain these parameters and improve predictive capabilities.

Using the given reservoir mineralogies and brine compositions (Table 3 and 4), a set of simulations is designed with three microbial rate

conditions as demonstrated in Table 5. Also, Table 6 shows the input parameters for the simulations. The “No Reaction” rate condition assumes no microbial activity occurs, the “High-Rate” condition uses the maximum values obtained from Refs. [34,46–51] and the “Moderate-Rate” conditions use the logarithmic average of the minimum and the maximum values in those references. There is a lack of kinetic data specific to UHS conditions, and the available values are primarily derived from lab-scale studies, which introduces uncertainty when applied to reservoir-scale simulations.

#### 3.2.1. A - Bentheimer Sandstone

The simulation results presented in Fig. 10 reveals that there is a significant difference under varying microbial conditions. The  $\text{H}_2$  mole fraction profiles (A–D panels in Fig 10) depicted during the injection and storage period indicate a substantial amount of  $\text{H}_2$  consumption due to microbial activities in high-rate conditions with approximately 34.82% of the injected  $\text{H}_2$  being consumed, compared to about 11.17% under moderate microbial conditions during the whole cycle. In all simulation cases, the amount of water saturation is high ( $S_w = 55\%$ ). If we consider a depleted gas reservoir where the residual water saturation is much less than this value (e.g. 15%), the amount of loss becomes around 3–4 times lower.

The  $\text{H}_2$  consumption rate profiles (E–H panels in Fig. 10) represent

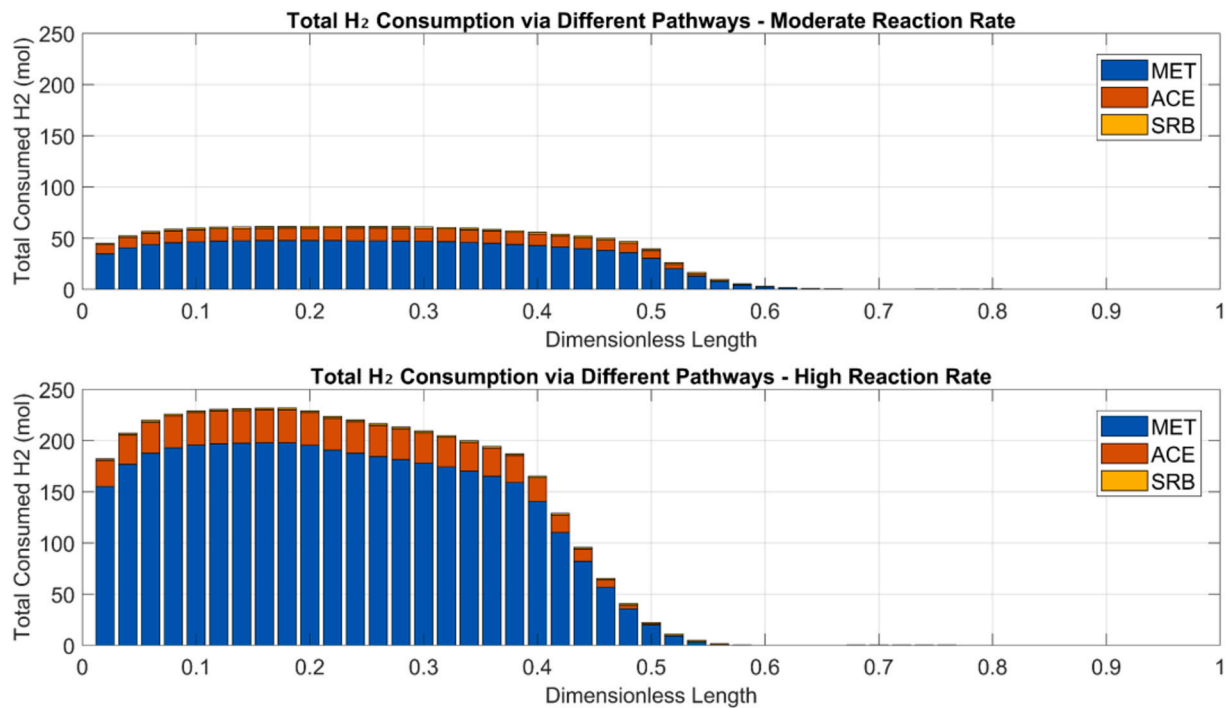


**Fig. 11.** The distribution of cumulative consumed H<sub>2</sub> during the whole cycle alongside with the reservoir in the Bentheimer Sandstone site. The total amount of injected H<sub>2</sub> is 13278.5 mol.

the rate of combined microbial H<sub>2</sub> consumption via MET, ACE, and SRB metabolisms. Over time, the consumption rate peaks and remains constant as long as there is enough reactant in the reservoir. Also, the predicted rates of H<sub>2</sub> consumption due to microbial activities are in the range of numbers that are reported in the Underground Sun Storage project in Austria ( $6.24 \frac{\text{mmol H}_2}{\text{L.day}}$ ) [52]. The pH profiles indicate an increase in all scenarios (I–L panels in Fig. 10); however, in the absence of microbial activity, the pH rise is attributed to water evaporation into the gas stream that has led to low amount of dolomite (CaMg(CO<sub>3</sub>)<sub>2</sub>) precipitation. In the presence of microbes, pH rises because of microbial reactions and a new equilibrium point due to the geochemical reactions. MET and ACE metabolisms consume HCO<sub>3</sub><sup>-</sup> and as a result they disrupt the equilibrium; therefore, dolomite starts to dissolve to compensate for bicarbonate consumption (M – P panels in Fig. 10). Concurrently, rising Ca<sup>2+</sup> and Mg<sup>2+</sup> levels trigger calcite and brucite (Mg(OH)<sub>2</sub>) precipitation while dolomite dissolution persists. In these simulations, changes in porosity and permeability were found to be minor. This outcome is consistent with a dolomite system, where dolomite dissolution is typically accompanied by the precipitation of calcite and brucite. Given their respective molar volumes—dolomite (6.44 cm<sup>3</sup>/mol), calcite (3.693 cm<sup>3</sup>/mol), and brucite (2.463 cm<sup>3</sup>/mol)—the net volume change is approximately  $-0.0284 \text{ cm}^3/\text{mol}$ , resulting in only a slight porosity increase. For instance, in these simulations, porosity increased from 0.2 to 0.200035. As a result, the associated change in permeability, calculated using the Carman–Kozeny formulation, was negligible. The pH level remains stabilised and buffered below 8 by these processes. The sustained pH level and the available HCO<sub>3</sub><sup>-</sup> allow ongoing microbial reactions, and thus the continuous H<sub>2</sub> consumption in the system.

The results presented in Fig. 11 show that microbial reactions happen more effectively a bit further from the wellbore. Close to the injection point, H<sub>2</sub> is highly available but water content is low due to displacement by the injected gas. Lower water correlates with lower cell numbers and limits microbial activity. In contrast, slightly further from the wellbore, there is H<sub>2</sub> for reactions and also more water. This combination creates ideal conditions for microbial growth and hydrogen consumption. At the front of the hydrogen plume, H<sub>2</sub> becomes limiting,

so microbial activity drops. Fig. 11 shows the total H<sub>2</sub> consumed via each metabolism during the entire injection, shut-in and withdrawal cycle and confirms that the highest H<sub>2</sub> loss occurs in the second region—where both H<sub>2</sub> and water content is high. This highlights that microbial activity, and thus H<sub>2</sub> consumption, is likely to be more pronounced where water hasn't yet been displaced, and hydrogen is present. Also, the activity of SRB metabolism is limited in this study as shown in Fig. 11 due to the lack of a continuous sulphate source. Since the mineralogies used do not contain sulphate minerals like anhydrite (CaSO<sub>4</sub>), the only available sulphate comes from the initial amount dissolved in water, restricting SRB activity across all cases.

### 3.2.2. B - Berea Sandstone

Figs. 12 and 13 present the simulation results during the injection and storage period in the Berea sandstone containing additional minerals of calcite and dolomite. In this storage site, the response is the same as for the Bentheimer sandstone. As discussed earlier, MET and ACE metabolisms need bicarbonate for the progress of reactions and dolomite dissolution can provide this. At the same time, calcite and brucite are precipitated resulting in buffering the environment and stabilizing pH near 8 (I–L panels in Fig. 12). This pH buffering effect allows microbial reactions to continue and consume H<sub>2</sub> in the reservoir. The H<sub>2</sub> consumption rate profiles (E–H panels in Fig. 12) show the summation of these three microbial reactions in the system. At early times, all microbial processes are active due to the availability of bicarbonate and sulphate in the system. As a result, the total H<sub>2</sub> consumption rate initially reaches approximately  $8 \text{ mmol H}_2 \cdot \text{kgw}^{-1} \cdot \text{day}^{-1}$  under moderate-rate conditions and around  $18 \text{ mmol H}_2 \cdot \text{kgw}^{-1} \cdot \text{day}^{-1}$  under high-rate conditions (See supplementary material section to access more data for simulations). Since there is not any other source of sulphate beyond the initially dissolved amount in the formation water (the formation mineralogy we used in this study does not have any sulphate source such as anhydrite), SRB activity gradually ceases over time (in all scenarios). The sharp rises and drops observed in the H<sub>2</sub> consumption rate profiles correspond to the existence/cessation of SRB metabolism, availability of bicarbonate, and H<sub>2</sub>. In panels E–H in Fig. 12, the sharp spike in hydrogen consumption rate near the H<sub>2</sub> plume front occurs

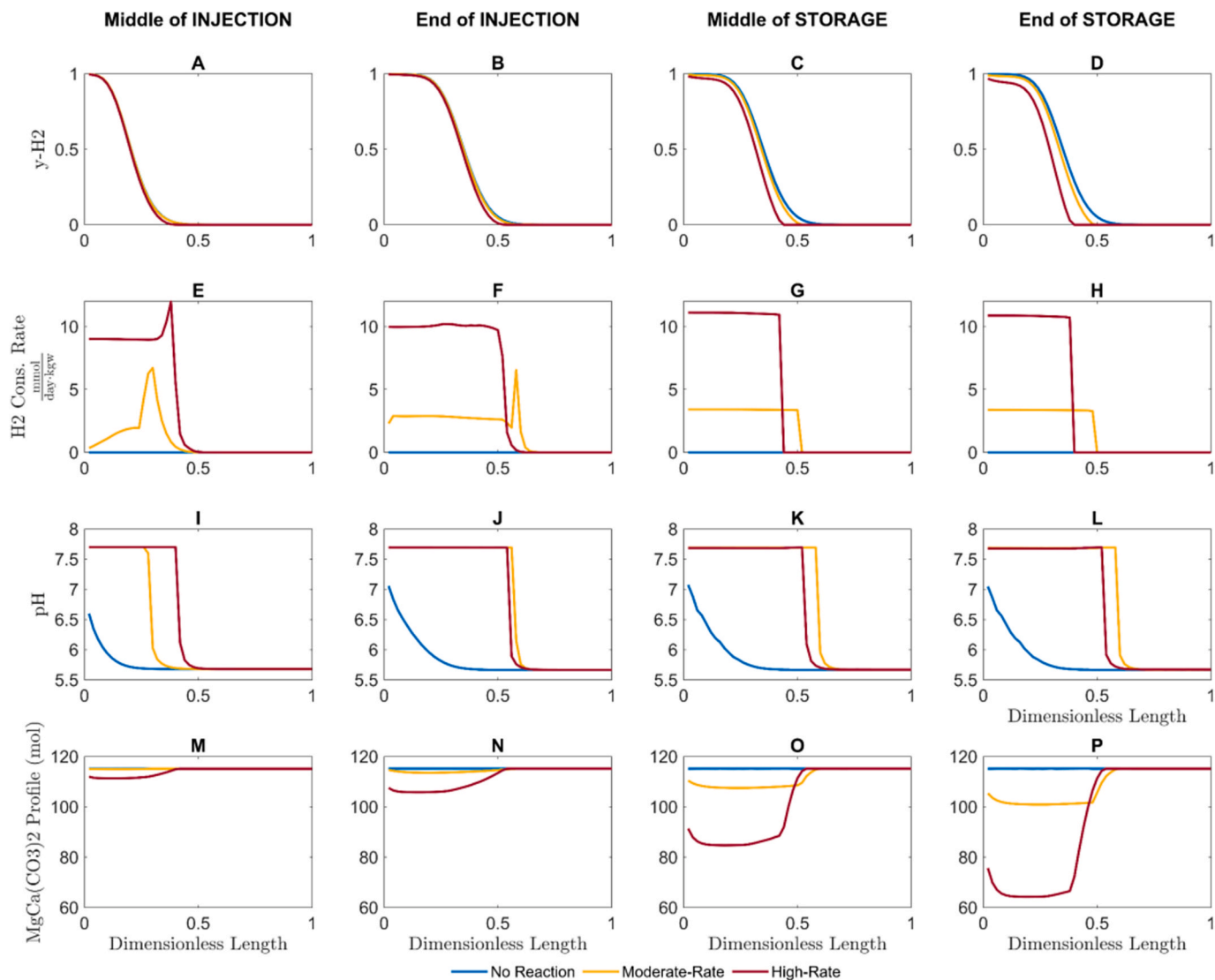


Fig. 12. Simulation results during the injection and storage period in site B with Berea sandstone.

because bicarbonate is initially abundant due to its pre-existing dissolved concentration in the reservoir brine. As MET and ACE metabolisms progress, bicarbonate is consumed and becomes limited. Since dolomite dissolution provides only a limited additional source, the reaction rate subsequently drops and stabilizes at a lower level. In the batch model where we specified the details of microbial and geochemical reactions [30], we assumed that there is a maximum population for microbes. When the population of microbes reaches the maximum value, the rate of reaction becomes constant. If you compare the  $y$ -H<sub>2</sub> profiles (mole fraction of H<sub>2</sub> in the gas phase, A–D panels in Fig. 12) with the reaction rate charts (panels E–H in Fig. 12), you will see that they are following each other and consistent.

Following this, MET and ACE become the dominant active pathways, resulting in a relatively stable and flat H<sub>2</sub> consumption rate during the remaining simulation period. Additionally, the H<sub>2</sub> consumption rate, pH, and dolomite profiles (E–P panels in Fig. 12) in the moderate-rate case indicate a broader region in the reservoir where microbial reactions occur. This is because, with slower microbial growth compared to the high-rate scenario, H<sub>2</sub> at the front has a longer residence time in the reservoir before significant microbial activity develops. As a result, H<sub>2</sub> penetrates deeper into the reservoir before being consumed, allowing reactions to take place over a more extended area.

In the high-rate condition, the rate of H<sub>2</sub> loss approaches nearly 11

mmol H<sub>2</sub>.kgw<sup>-1</sup>.day<sup>-1</sup>, which is nearly two times greater than the value reported in the Underground Sun Storage project [52]. In this simulation, in the high-rate condition and moderate-rate condition, 35.19% and 13.27% of injected H<sub>2</sub> was consumed by microbes during the whole cycle, respectively.

### 3.2.3. C - Grey Berea Sandstone

The storage performance in the storage site C with the Grey Berea sandstone mineralogy is depicted in Figs. 14 and 15. The H<sub>2</sub> concentration profiles (A–D panels in Fig. 14) during injection and storage suggest that there are no significant reactions in the system, as there is no significant deviation from the “No Reaction” condition. The consumption rate profiles (E–H panels in Fig. 14) indicate that initially there are some reactions, but, over time, the rate of H<sub>2</sub> consumption decreases to zero, indicating the cessation of microbial reactions. This behavior can be attributed to the pH change. If calcite is the only mineral in a carbonate system, pH increases when calcite starts to dissolve. Since the rate of microbial reactions is dependent on pH, microbial reactions stop when the pH reaches the upper limit. This pH is above the assumed maximum limit for methanogens and acetogens [21] and the microbial reactions will eventually stop. In this scenario, the availability of carbonate for MET and ACE metabolisms is restricted to the initial dissolved carbonate and a limited contribution from calcite dissolution. Since the

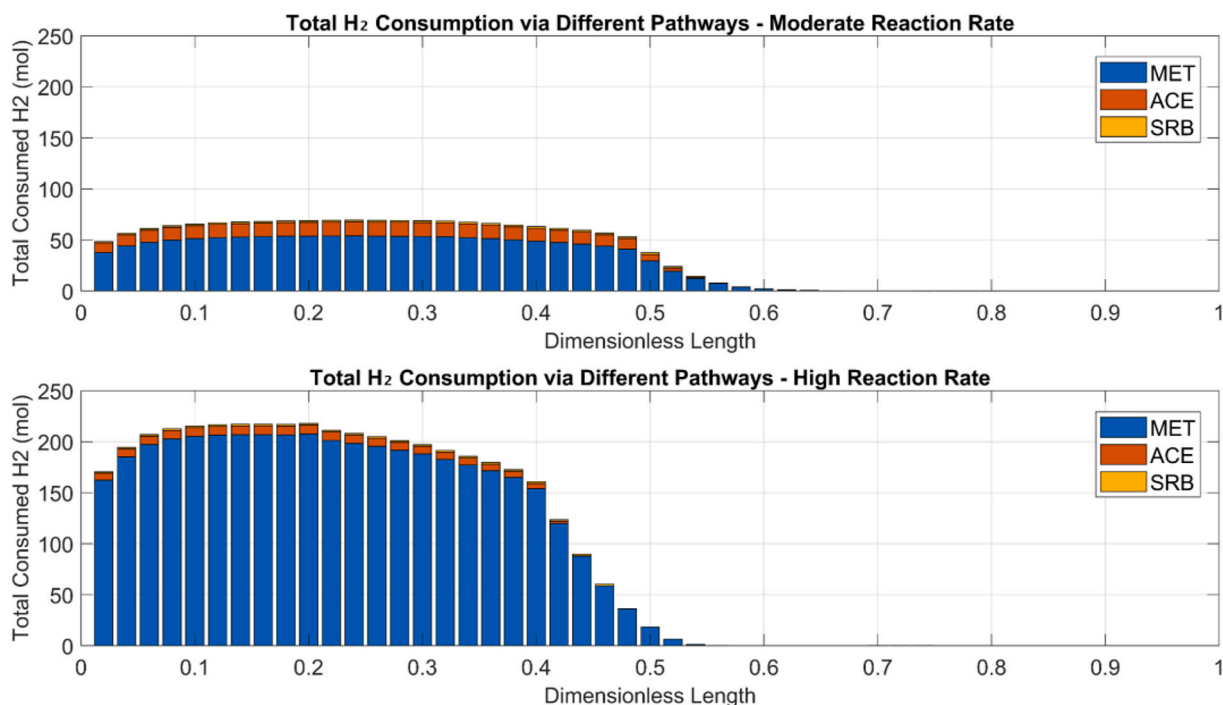


**Fig. 13.** The distribution of cumulative consumed H<sub>2</sub> during the whole cycle alongside with the reservoir in the Berea Sandstone site. The total amount of injected H<sub>2</sub> is 13278.5 mol.

MET metabolism proceeds at a faster rate than ACE, it outcompetes ACE, inhibiting the growth of ACE microbes in the high-rate scenario, as shown in Fig. 15.

The calcite dissolution/precipitation profiles (M – P panels in Fig. 14) show that dissolution is stopped compared to previous cases due to the rise in pH and the cessation of microbial reactions. This indicates that the initial reactions might have consumed some H<sub>2</sub>, but as the pH increases due to calcite dissolution, microbial activity decreases, leading to the stabilization of the system. This pH behavior aligns with findings from Dopffel et al. [23], who reported that microbial hydrogen consumption under high-saline conditions leads to significant pH increases.

The overall implication is that in the presence of only calcite (and absence of dolomite), the system is limiting microbial activity and therefore preventing extensive H<sub>2</sub> consumption and maintaining storage integrity. This behavior ensures the long-term stability of H<sub>2</sub> storage in Grey Berea sandstone, making it a viable option for underground H<sub>2</sub> storage applications. In this case, in the high-rate condition and moderate condition, 5.98% and 5.94% of injected H<sub>2</sub> was consumed by microbes, respectively.

#### 4. Future works

Modeling microbial processes in the subsurface is inherently challenging due to the complexity and diversity of microbial life. Each metabolic pathway can involve numerous species of Archaea and Bacteria, each with potentially different kinetic behaviours. In this study, we simplified this complexity by representing each metabolism with a single microbial group, which inevitably limits the biological realism of the model. Capturing the full spectrum of microbial diversity while also solving for multiphase flow in porous media presents a substantial computational and conceptual challenge. It is important to note that this model does not currently account for porosity reduction due to microbial activity such as biofilm growth or pore clogging, which could become more significant in long-term or high-biomass scenarios and will be considered in future work. Another major limitation is the scarcity of reliable kinetic data. Parameters such as specific growth rates and half-saturation constants are critical for accurate modeling, yet they are often

poorly constrained, especially under reservoir conditions. Performing more laboratory tests under in-situ temperature and pressure in porous media to obtain these values is essential. To better capture the reality of microbial reactions during UHS, future work should also involve pilot-scale field tests and history matching techniques. These approaches can help estimate the extent and severity of microbial activity under realistic operational scenarios.

This framework simulates UHS by integrating a range of input parameters, including storage cycle scenarios, spatial mineralogy distribution, brine composition, and microbial reaction kinetics. We acknowledge the significant challenges in predicting bio-geochemical reactions coupled with flow dynamics, and our goal is to provide a robust numerical framework as a foundation for ongoing improvement. We welcome collaborations that involve laboratory or pilot-scale testing to support further validation and refinement of this model.

#### 5. Conclusions

During this study a reactive transport model that is suitable for UHS was developed. The model, named Underground Gas Flow Simulations with Coupled Bio-Geochemical Reactions (or UGFACT) was developed by coupling PHREEQC software and the compositional module in MRST. The UGFACT model was verified by comparing the model outputs with two commercial compositional reservoir simulators (E300 and CMG-GEM). The benchmarking results demonstrated an excellent agreement between our model and the commercial software in terms of fluid flow and geochemistry in a CO<sub>2</sub> storage trial. Then, the UGFACT model was employed to conduct a calculation of a simple H<sub>2</sub> storage cycle in three given rock mineralogies with three different microbial conditions, leading to the following results:

- The model suggests that within Bentheimer sandstone and Berea sandstone reservoirs microbial H<sub>2</sub> consumption can occur with a strong influence of the presence of buffering minerals. Given conditions and assumptions in the high-rate case, up to 36% of injected H<sub>2</sub> may be consumed in the configured system while in the moderate rate it is close to 14%.

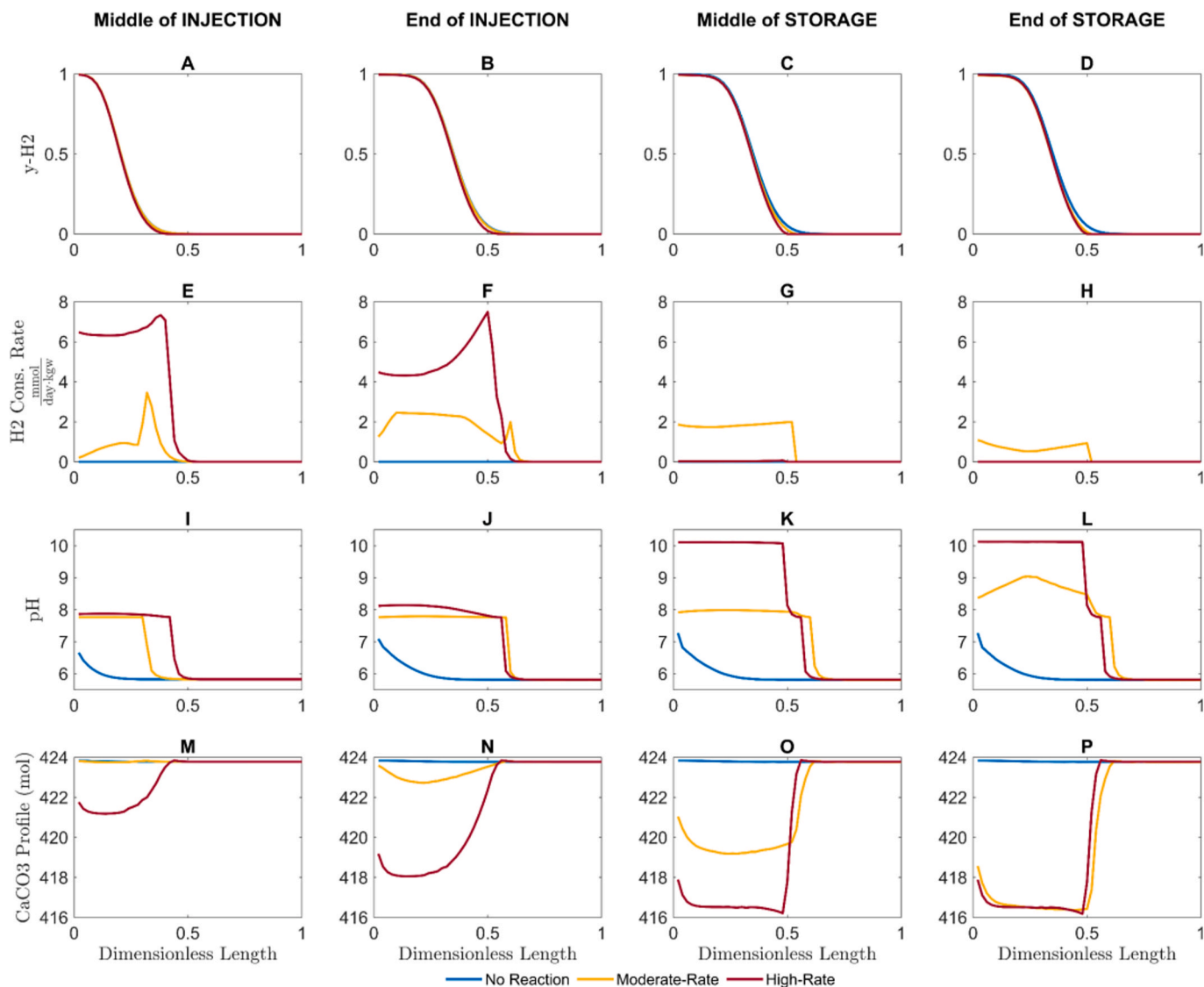


Fig. 14. Simulation results during the injection and storage period in site C with Grey Berea sandstone.

- The results indicate that the reservoir with Grey Berea sandstone, which in our case did not contain significant amounts of buffering minerals (only calcite is present), is less sensitive to microbial H<sub>2</sub> consumption reactions. In other words, with the given conditions and assumptions, the pH will quickly increase and limit further microbial H<sub>2</sub> consumption.
- The model suggests that the presence of dolomite in the reservoir can play a key role by providing a carbon source for MET and ACE, resulting in H<sub>2</sub> loss due to microbial activities, while keeping pH favourable for microbes.
- The model predicts that under the worst-case scenario (the most favourable condition for microbes), the upper limit of the H<sub>2</sub> consumption rate via MET and ACE is around  $11 \frac{\text{mmol H}_2}{\text{kgw.day}}$  (milli moles of H<sub>2</sub> per kilogram of water per day) based on the kinetic parameters used.
- In sandstone reservoirs, secondary minerals (carbonates) can be key factors influencing hydrogen consumption.
- Our primary objective is to develop a rigorous numerical tool to address these complexities, but it is clear that significant challenges are associated with predicting bio-geochemical reactions coupled with flow dynamics. More experimental and field data is needed to improve the model predictions.

- Given the wide range of potential biochemical reactions in subsurface environments, more experimental data on reaction kinetics are urgently needed to accurately assess risks and develop effective mitigation strategies for UHS.

#### CRedit authorship contribution statement

**A. Shojaee:** Writing – review & editing, Writing – original draft, Visualization, Validation, Software, Methodology, Investigation, Formal analysis, Data curation, Conceptualization. **S. Ghanbari:** Writing – review & editing, Supervision, Project administration, Methodology, Investigation, Formal analysis, Conceptualization. **G. Wang:** Writing – review & editing, Supervision, Project administration, Methodology, Investigation, Formal analysis, Conceptualization. **S. Gregory:** Writing – review & editing, Conceptualization. **N. Dopffel:** Writing – review & editing, Conceptualization. **E. Mackay:** Writing – review & editing, Supervision, Resources, Project administration, Methodology, Funding acquisition, Formal analysis, Conceptualization.

#### Declaration of competing interest

The authors declare that they have no known competing financial

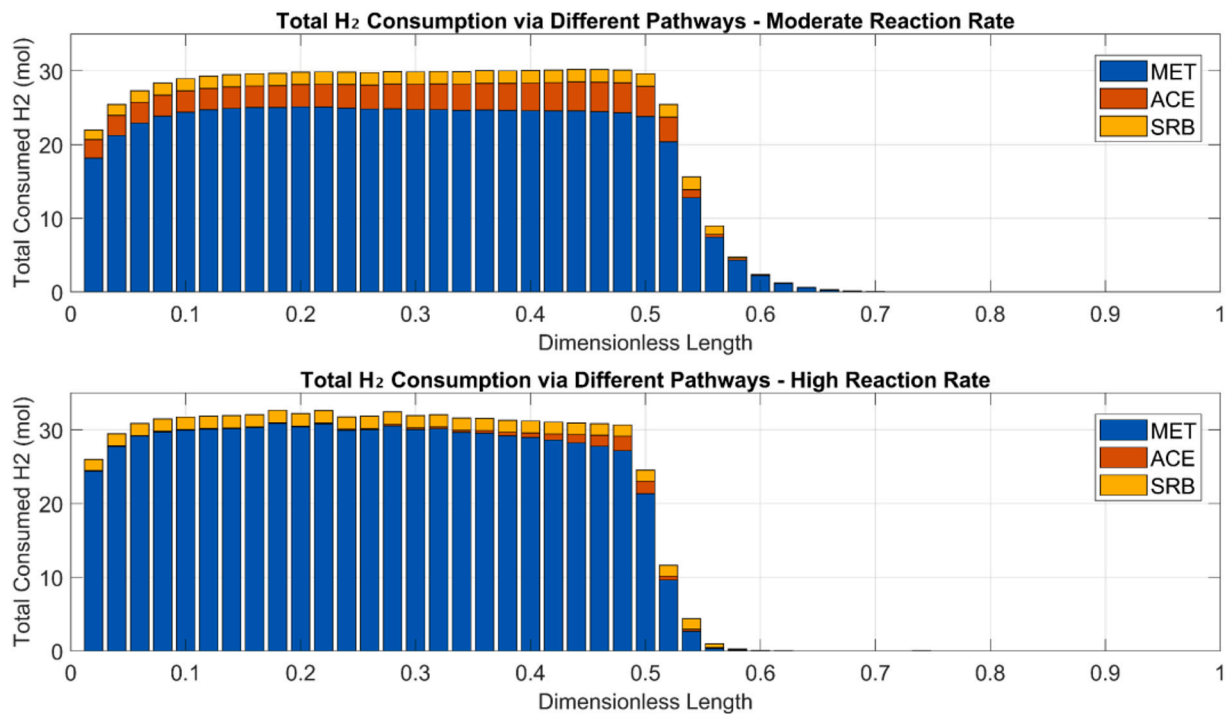


**Fig. 15.** The distribution of cumulative consumed H<sub>2</sub> during the whole cycle alongside with the reservoir in the Grey Berea Sandstone site. The total amount of injected H<sub>2</sub> is 13278.5 mol.

interests or personal relationships that could have appeared to influence the work reported in this paper.

### Acknowledgements

The authors extend their gratitude to the James Watt Scholarship programme at Heriot-Watt University for sponsoring this project. Additionally, we would like to acknowledge the Energi Simulation Foundation for funding the Chair in CCUS and Reactive Flow Simulation, held by Eric Mackay. We extend our gratitude to the iNetZ + Global Research Institute at Heriot-Watt University for their support of Dr Gang Wang's research on Underground Hydrogen Storage in his capacity as theme lead. CMG Ltd are thanked for use of the GEM reservoir simulator, and SLB are thanked for use of the E300 reservoir simulator. Simon Gregory publishes this manuscript with the permission of the Executive Director of the British Geological Survey and funded by the British Geological Survey via NERC national capability. N. Dopffel acknowledges funding through the MOCHyS project (RCN project no 344183).

### Appendix A. Supplementary data

Supplementary data to this article can be found online at <https://doi.org/10.1016/j.ijhydene.2025.150453>.

### Data availability

The simulation module developed in this study, UGFACT (Underground Gas Flow simulAtions with Coupled bio-geochemical reacTions), has been released as an open-source framework. It integrates MRST with PHREEQC to model reactive transport involving microbial and geochemical reactions in porous media. The full implementation, including example cases and setup instructions, is available at: <https://github.com/ahmadrezashojaee/UGFACT>.

### References

- [1] Elam CC, Padró CEG, Sandrock G, Luzzi A, Lindblad P, Hagen EF. Realizing the hydrogen future: the International Energy Agency's efforts to advance hydrogen energy technologies. *Int J Hydrogen Energy* 2003;06/01/2003;28(6):601–7. [https://doi.org/10.1016/S0360-3199\(02\)00147-7](https://doi.org/10.1016/S0360-3199(02)00147-7).
- [2] Zeng L, Sander R, Chen Y, Xie Q. Hydrogen storage performance during underground hydrogen storage in depleted gas reservoirs: a review. *Engineering* 2024;04/12/2024. <https://doi.org/10.1016/j.eng.2024.03.011>.
- [3] Jahanbakhsh A, Louis Potapov-Crighton A, Mosallanezhad A, Tohidi Kaloorazi N, Maroto-Valer MM. Underground hydrogen storage: a UK perspective. *Renew Sustain Energy Rev* 2024;01/01/2024;189:114001. <https://doi.org/10.1016/j.rser.2023.114001>.
- [4] Tackie-Otoo BN, Haq MB. A comprehensive review on geo-storage of H<sub>2</sub> in salt caverns: prospect and research advances. *Fuel* 2024;01/15/2024;356:129609. <https://doi.org/10.1016/j.fuel.2023.129609>.
- [5] Thiagarajan SR, Emadi H, Hussain A, Patange P, Watson M. A comprehensive review of the mechanisms and efficiency of underground hydrogen storage. *J Energy Storage* 2022;07/01/2022;51:104490. <https://doi.org/10.1016/j.est.2022.104490>.
- [6] Hassannayebi N, Azizmohammadi S, De Lucia M, Ott H. Underground hydrogen storage: application of geochemical modelling in a case study in the Molasse Basin, Upper Austria. *Environ Earth Sci* 2019;02/28 2019;78(5):177. <https://doi.org/10.1007/s12665-019-8184-5>.
- [7] Wu L, et al. Site selection for underground bio-methanation of hydrogen and carbon dioxide using an integrated multi-criteria decision-making (MCDM) approach. *Energy* 2024;10/15/2024;306:132437. <https://doi.org/10.1016/j.energy.2024.132437>.
- [8] Zivar D, Kumar S, Foroozesh J. Underground hydrogen storage: a comprehensive review. *Int J Hydrogen Energy* 2021;07/01/2021;46(45):23436–62. <https://doi.org/10.1016/j.ijhydene.2020.08.138>.
- [9] Camargo JT, White JA, Hamon FP, Fakeye V, Buscheck TA, Huerta N. Managing reservoir dynamics when converting natural gas fields to underground hydrogen storage. *Int J Hydrogen Energy* 2024;01/02/2024;49:1261–73. <https://doi.org/10.1016/j.ijhydene.2023.09.165>.
- [10] Tarkowski R. Underground hydrogen storage: characteristics and prospects. *Renew Sustain Energy Rev* 2019;05/01/2019;105:86–94. <https://doi.org/10.1016/j.rser.2019.01.051>.
- [11] Wang G, Pickup G, Sorbie K, Mackay E. Numerical modelling of H<sub>2</sub> storage with cushion gas of CO<sub>2</sub> in subsurface porous media: filter effects of CO<sub>2</sub> solubility. *Int J Hydrogen Energy* 2022;08/05/2022;47(67):28956–68. <https://doi.org/10.1016/j.ijhydene.2022.06.201>.
- [12] Wang G, Pickup G, Sorbie K, Mackay E. Scaling analysis of hydrogen flow with carbon dioxide cushion gas in subsurface heterogeneous porous media. *Int J Hydrogen Energy* 2022;01/08/2022;47(3):1752–64. <https://doi.org/10.1016/j.ijhydene.2021.10.224>.

- [13] Perera MSA. A review of underground hydrogen storage in depleted gas reservoirs: insights into various rock-fluid interaction mechanisms and their impact on the process integrity. *Fuel* 2023/02/15/2023;334:126677. <https://doi.org/10.1016/j.fuel.2022.126677>.
- [14] Abdellatif M, Hashemi M, Azizmohammadi S. Large-scale underground hydrogen storage: integrated modeling of reservoir-wellbore system. *Int J Hydrogen Energy* 2023/06/12/2023;48(50):19160–71. <https://doi.org/10.1016/j.ijhydene.2023.01.227>.
- [15] Tarkowski R, Uliasz-Misiak B. Towards underground hydrogen storage: a review of barriers. *Renew Sustain Energy Rev* 2022/07/01/2022;162:112451. <https://doi.org/10.1016/j.rser.2022.112451>.
- [16] Dopffel N, Jansen S, Gerritse J. Microbial side effects of underground hydrogen storage – knowledge gaps, risks and opportunities for successful implementation. *Int J Hydrogen Energy* 2021/02/16/2021;46(12):8594–606. <https://doi.org/10.1016/j.ijhydene.2020.12.058>.
- [17] Ebigo A, Golfier F, Quintard M. A coupled, pore-scale model for methanogenic microbial activity in underground hydrogen storage. *Adv Water Resour* 2013/11/01/2013;61:74–85. <https://doi.org/10.1016/j.advwatres.2013.09.004>.
- [18] Wang G, Pickup G, Sorbie K, de Rezende JR, Zarei F, Mackay E. Bioreaction coupled flow simulations: impacts of methanogenesis on seasonal underground hydrogen storage. *Int J Hydrogen Energy* 2024/02/15/2024;55:921–31. <https://doi.org/10.1016/j.ijhydene.2023.11.035>.
- [19] Safari Z, Fatehi R, Azin R. Developing a numerical model for microbial methanation in a depleted hydrocarbon reservoir. *Renew Energy* 2024/06/01/2024;227:120426. <https://doi.org/10.1016/j.renene.2024.120426>.
- [20] Wang G, Pickup G, Sorbie K, Mackay E. Numerical analysis of bio-methanation process during underground hydrogen storage, 2022; 2022. p. 1–5. <https://doi.org/10.3997/2214-4609.202221058>. 1.
- [21] Thaysen EM, et al. Estimating microbial growth and hydrogen consumption in hydrogen storage in porous media. *Renew Sustain Energy Rev* 2021/11/01/2021;151:111481. <https://doi.org/10.1016/j.rser.2021.111481>.
- [22] Muhammed NS, Haq MB, Al Shehri D, Amao A. Comparative study on hydrogen losses via microbial byproduct in the presence of methane and nitrogen cushion gas. *Int J Hydrogen Energy* 2024/09/04/2024;81:237–48. <https://doi.org/10.1016/j.ijhydene.2024.07.272>.
- [23] Dopffel N, et al. Microbial hydrogen consumption leads to a significant pH increase under high-saline-conditions: implications for hydrogen storage in salt caverns. *Sci Rep* 2023/06/29 2023;13(1):10564. <https://doi.org/10.1038/s41598-023-37630-y>.
- [24] Muhammed NS, Haq B, Al Shehri D, Al-Ahmed A, Rahman MM, Zaman E. A review on underground hydrogen storage: insight into geological sites, influencing factors and future outlook. *Energy Rep* 2022/11/01/2022;8:461–99. <https://doi.org/10.1016/j.egy.2021.12.002>.
- [25] Gao Q, Liu J, Elsworth D. Phenomenal study of microbial impact on hydrogen storage in aquifers: a coupled multiphysics modelling. *Int J Hydrogen Energy* 2024/08/19/2024;79:883–900. <https://doi.org/10.1016/j.ijhydene.2024.07.004>.
- [26] Vítězová M, et al. In situ field experiment shows the potential of methanogenic archaea for biomethane production from underground gas storage in natural rock environment. *Environ Technol Innov* 2023/11/01/2023;32:103253. <https://doi.org/10.1016/j.eti.2023.103253>.
- [27] Hogeweg S, Hagemann B, Bobrov V, Ganzer L. Development and calibration of a bio-geo-reactive transport model for UHS. *Front Energy Res Original Res* 2024-May-15 2024;12. <https://doi.org/10.3389/fenrg.2024.1385273> (in English).
- [28] Minougou JD, Azizmohammadi S, Gholami R, Ott H. A bio-reactive transport model for biomethanation in hydrogen underground storage sites. *Greenhouse Gases: Sci Technol* 2024;14(6):977–94. <https://doi.org/10.1002/ghg.2307>.
- [29] Jahanbani Veshareh M, Thaysen EM, Nick HM. Feasibility of hydrogen storage in depleted hydrocarbon chalk reservoirs: assessment of biochemical and chemical effects. *Appl Energy* 2022/10/01/2022;323:119575. <https://doi.org/10.1016/j.apenergy.2022.119575>.
- [30] Shojaee A, Ghanbari S, Wang G, Mackay E. Interplay between microbial activity and geochemical reactions during underground hydrogen storage in a seawater-rich formation. *Int J Hydrogen Energy* 2024/01/02/2024;50:1529–41. <https://doi.org/10.1016/j.ijhydene.2023.10.061>.
- [31] Shojaee A, Ghanbari S, Wang G, Mackay E. Integrated modelling of bio-geochemical aspects in underground hydrogen storage: implications for reservoir selection and performance. In: Presented at the SPE europe energy conference and exhibition; 2024. <https://doi.org/10.2118/220056-MS> [Online]. Available:
- [32] Parkhurst D, Appelo T. User's guide to PHREEQC version 3 - a computer program for speciation, batch-reaction, one-dimensional transport, and inverse geochemical calculations. 1999.
- [33] Parkhurst DL. *User's guide to PHREEQC : a computer program for speciation, reaction-path, advective-transport, and inverse geochemical calculations*. Lakewood, Colo. : U.S. Dept. of the Interior, U.S. Geological Survey ; Denver, CO : earth Science Information Center, Open-File Reports Section [distributor], 1995. 1995.
- [34] Smeaton CM, Van Cappellen P. Gibbs energy dynamic yield method (GEDYM): predicting microbial growth yields under energy-limiting conditions. *Geochem Cosmochim Acta* 2018/11/15/2018;241:1–16. <https://doi.org/10.1016/j.gca.2018.08.023>.
- [35] Monod J. The growth of bacterial cultures. *Annu Rev Microbiol* 1949/10/01 1949;3(1):371–94. <https://doi.org/10.1146/annurev.mi.03.100149.002103>.
- [36] Liu S. Chapter 11 - how cells grow. In: Liu S, editor. *Bioprocess engineering*. second ed. Elsevier; 2017. p. 629–97.
- [37] Liu S. Chapter 12 - cell cultivation. In: Liu S, editor. *Bioprocess engineering*. second ed. Elsevier; 2017. p. 699–782.
- [38] Lie K-A. An introduction to reservoir simulation using MATLAB/GNU octave: user guide for the MATLAB reservoir simulation Toolbox (MRST). Cambridge: Cambridge University Press; 2019.
- [39] Lie K-A, Møyner O. *Advanced modeling with the MATLAB reservoir simulation Toolbox*. Cambridge: Cambridge University Press; 2021.
- [40] Shojaee A, Kord S, Miri R, Mohammadzadeh O. Reactive transport modeling of scale precipitation and deposition during incompatible water injection in carbonate reservoirs. *J Pet Explor Prod Technol* 2024/02/01 2024;14(2):515–34. <https://doi.org/10.1007/s13202-023-01715-1>.
- [41] Wang G, Pickup GE, Sorbie KS, Mackay EJ. Analysis of compositional effects on global flow regimes in CO<sub>2</sub> near-miscible displacements in heterogeneous systems. *Transport Porous Media* 2019/09/01 2019;129(3):743–59. <https://doi.org/10.1007/s11242-019-01304-z>.
- [42] Strobel G, Hagemann B, Lüddecke CT, Ganzer L. Coupled model for microbial growth and phase mass transfer in pressurized batch reactors in the context of underground hydrogen storage. *Front Microbiol Original Res* 2023-April-04 2023;14. <https://doi.org/10.3389/fmicb.2023.1150102> (in English).
- [43] Al-Muntasheri GA, Zitha PLJ, Nasr-El-Din HA. A new organic gel system for water control: a computed tomography study. *SPE J* 2009;15(1):197–207. <https://doi.org/10.2118/129659-PA>.
- [44] Mahmoud MAA, Nasr-El-Din HAA, de Wolf CAA. High-temperature laboratory testing of illitic sandstone outcrop cores with HCl-alternative fluids. *SPE Prod Oper* 2015;30(1):43–51. <https://doi.org/10.2118/147395-PA>.
- [45] Shehata AM, Nasr-El-Din HA. Role of sandstone mineral compositions and rock quality on the performance of low-salinity waterflooding. In: Presented at the international petroleum technology conference; 2014. <https://doi.org/10.2523/IPTC-18176-MS> [Online]. Available:
- [46] Lovley Derek R, Dwyer Daryl F, Klug Michael J. Kinetic analysis of competition between sulfate reducers and methanogens for hydrogen in sediments. *Appl Environ Microbiol* 1982;43(6):1373–9. <https://doi.org/10.1128/aem.43.6.1373-1379.1982/06/01> 1982.
- [47] Dornseiffer P, Meyer B, Heinze E. Modeling of anaerobic formate kinetics in mixed biofilm culture using dynamic membrane mass spectrometric measurement. *Biotechnol Bioeng* 1995/02/05 1995;45(3):219–28. <https://doi.org/10.1002/bit.260450306>.
- [48] Stams AJM, Elferink SJWHO, Westermann P. In: *Biomethanation I*, Ahring BK, et al., editors. *Metabolic interactions between methanogenic consortia and anaerobic respiring bacteria*. Berlin, Heidelberg: Springer Berlin Heidelberg; 2003. p. 31–56.
- [49] Khanal SK. *Anaerobic biotechnology for bioenergy production: principles and applications*. 2008i–xv.
- [50] Kotsyurbenko OR, Glagolev MV, Nozhevnikova AN, Conrad R. Competition between homoacetogenic bacteria and methanogenic archaea for hydrogen at low temperature. *FEMS (Fed Eur Microbiol Soc) Microbiol Ecol* 2001;38(2–3):153–9. <https://doi.org/10.1111/j.1574-6941.2001.tb00893.x>.
- [51] Pallud C, Van Cappellen P. Kinetics of microbial sulfate reduction in estuarine sediments. *Geochem Cosmochim Acta* 2006/03/01/2006;70(5):1148–62. <https://doi.org/10.1016/j.gca.2005.11.002>.
- [52] Hellerschmied C, et al. Hydrogen storage and geo-methanation in a depleted underground hydrocarbon reservoir. *Nat Energy* 2024/03/01 2024;9(3):333–44. <https://doi.org/10.1038/s41560-024-01458-1>.